ELSEVIER

Physica C 307 (1998) 165–176

PHYSICA C

Local magnetization measurements on $Bi_2Sr_2Ca_2Cu_3O_{10}$ tapes

Y. Radzyner [a,*], Y. Abulafia [a], Y. Yeshurun [a], T. Staiger [b], G. Fuchs [b]

[a] *Institute of Superconductivity, Department of Physics, Bar-Ilan University, Ramat-Gan 52900, Israel*
[b] *Institut für Festkörper-und Werkstofforschung Dresden, Postfach 270016, D-01171 Dresden, Germany*

Received 16 June 1998; revised 19 August 1998; accepted 2 September 1998

Abstract

Global transport measurements and local Hall-probe array measurements of a section of silver clad BSCCO tape, are reported. Transport measurements are in good agreement with the 'brick wall' model. The induction profiles obtained from magnetic measurements agree with the assumption of a uniform bulk current at low (40–60 K) temperatures. At higher temperatures and relatively high fields (700 G and up) local measurements seem to reveal the existence of surface currents. These currents are the result of small current loops, flowing within the grains, which result in a net current only at the edges of the sample. Thus, the local magnetic measurements do not agree with global transport ones, and we contend that the 'brick wall' model aptly describes the flow of transport currents, but fails to describe the flow of currents induced by an external magnetic field.

PACS: 74.72 Hs; 74.80 Bj; 74.60 Jg; 74.60 Ge

Keywords: Weak links; Critical current density; Local measurements; Magnetic measurements; Granular material; Flux creep

1. Introduction

Significant progress has been made in the development of long silver sheathed $(Bi,Pb)_2Sr_2Ca_2Cu_3O_{10}$ (Bi-2223) tapes using the 'powder in tube' technique. In multifilamentary Bi-2223/Ag tapes with lengths up to 1500 m, high critical current densities up to 25 kA/cm^2 have been achieved at 77 K in zero magnetic field [1–3].

The critical current density of Bi-2223/Ag tapes in magnetic fields is limited by strong flux creep of pancake vortices resulting in a very low irreversibility field at 77 K. Different attempts to introduce strong pinning defects by irradiation techniques have been reported [4,5], but the irreversibility field could be enhanced only up to about 1.5 T at 77 K. Thus, the field and temperature dependence of the critical current density at high and medium temperatures and not too low magnetic fields is affected by the activation energy for flux creep. At lower temperatures, the influence of flux creep effects on the critical current density is reduced and the granularity of the textured polycrystalline material limits the current carrying capability of the tapes.

Two models are commonly used to describe the flow of current in granular materials, the 'railway switch' [6] and the 'brick wall' model [7–9]. For morphological reasons, which will be discussed later, only the brick wall model is pertinent to our data.

* Corresponding author. Tel.: +972-3-531-8433; Fax: +972-3-535-3298; E-mail:radzyner@mail.biu.ac.il

0921-4534/98/$ - see front matter
PII: S0921-4534(98)00514-0

This model suggests that in a region of low fields applied perpendicular to the surface of the tape, some of the weak links within the *ab* planes break and the current detours through links parallel to the *c*-axis [9]. Two different coupling strengths of *c*-axis boundaries between the grains were assumed: weak-linked and strong-linked grains. Whereas the critical current density of the strong-linked grains is larger than the intra-grain critical current density in the whole field range, the weak-linked grains are for not too high applied fields the bottleneck, which imposes the limit for the current. Once the current exceeds this limit, a kink appears in the $j_c(B)$ curve at low magnetic field. The model predicts the appearance of a second kink at a higher magnetic field. Above this field, the transport current is limited by flux creep in the grains resulting in a strong, exponential $j_c(B)$ dependence. Using this scenario of the 'brick wall' model, for a quantitative analysis of experimental $j_c(B,T)$ curves of Bi-2223/Ag tapes, it has been found that at low temperatures only a small fraction of well coupled grains of about 10% is effective to provide high critical current densities [10,11].

The microstructure of the tapes shows in large regions of the material stacks of platelet-shaped grains with common *c*-axis separated by twist boundaries, so called 'colonies'. Whereas near the silver sheath the 'colonies' are almost perfectly aligned with the Ag over long distances, different types of boundaries between adjacent 'colonies' are observed inside the tapes, where the alignment of the 'colonies' is much poorer than in the region near the silver sheath. The consequences of this different character of the microstructure on the current transport have been investigated by magneto-optical techniques. Small current loops were observed inside the tapes, whereas large current loops are induced near the silver sheath [12].

A non-uniform current distribution has been found not only across the thickness of the superconducting core but also in the plane of the tape. This lateral current distribution has been investigated by movable miniature Hall sensor measurements [13] and by cutting slices in the tapes [14,15]. A critical current density of 76 kA/cm^2 at 77 K has been measured for a central slice of a tape having an overall critical current density of about 13 kA/cm^2 [14]. These results demonstrate the local variation of the critical current density in the tape in length scales of 100 μm width and 5–10 μm thickness, which are typical for segments extracted from the tapes.

Recently, an experimental technique was developed for the study of the local variation of magnetic induction in much smaller length scales of several μm [16]. Arrays of miniature Hall sensors were used for local magnetization measurements of $YBa_2Cu_3O_{7-\delta}$ [17,18] and $Bi_2Sr_2CaCu_2O_8$ single crystals [19]. Applying this technique on individual Bi-2223 grains or 'colonies' would allow studying the intrinsic properties of the basic elements for the current transport in the Bi-2223 tapes. In the present paper, small samples cut from a Bi-2223/Ag tape have been studied by local magnetization.

2. Experimental

Silver sheathed Bi-2223 tapes were produced by the 'powder in tube' technique as described in [20]. Monofilamentary samples of approximately 3 mm width and 90 μm thickness were obtained. The superconducting core showed a roughly elliptical cross-section with a typical width of 2.2 mm and a thickness of 40 μm. Samples of about 15 mm length were cut from the rolled tapes. They were investigated by transport measurements in the temperature range between 4.2 K and 77 K and in magnetic fields up to 12 T and showed typical values of the critical current density of 25 kA/cm^2 at 77 K in self field. The critical current was determined at an electric field criterion of 0.1 μV/cm.

To expose the superconducting core without damage, epoxy stripes of 0.5 mm thickness were glued on both broad sides of the tape. The whole sandwich was sliced in longitudinal direction by a wire saw in three stripes of about 1 mm width. Finally, the top and the bottom part of the central slice were separated carefully. The superconducting layers of both parts showed a uniform thickness of about 20 μm along the whole sample length, in contrast to the result of Lelovic et al. [21] who observed in a similar splitting experiment a strongly asymmetric separation of the core. In order to investigate the influence of this splitting technique on the critical current density, we produced a central slice of 2 mm width and separated it carefully. The critical current density

of the top and bottom parts showed the same values as an unpeeled slice of 1 mm width within an accuracy of 5% in the whole temperature and field range.

Small samples (2 mm × 0.8 mm) were extracted by two parallel cuts from longer samples prepared as described before. Local magnetization measurements were performed on such samples using an array of 11 GaAs/AlGaAs Hall sensors with $30 \times 30\ \mu m^2$ active area. After zero-field cooling the sample to the measurement temperature, all Hall miniature sensors measured the hysteresis loops of local magnetization (B_z–H). The probes detect the component B_z of the field normal to the surface of the sample. From the experimental data, the field profiles $B_z(x)$ were determined for various applied fields on the ascending and descending branches of $B_z(H)$.

3. Results and discussion

3.1. Characterization of tapes by transport measurements

In Fig. 1 the critical current density of a monocore Bi-2223/Ag tape is shown as a function of magnetic field for different temperatures. The $j_c(B)$ curves are separated by two kinks. The first kink, separating a very narrow region of extremely high critical currents at very low magnetic fields, is indicated by a thick arrow in Fig. 1. The second kink separates two regions with two distinct slopes in the region of high magnetic fields and low critical currents (see e.g., kink in the data obtained at 35 K, which is pointed to by a thin arrow).

In the region above the higher kink, the current flows through the bulk, crossing links in the *ab* planes. The kink indicates that the links within the planes break, and the current follows the 'brick-wall' model [7–9], in which the current detours through links parallel to the *c*-axis. The lower kink at higher fields indicates that the critical transport current is limited by flux creep in the grains. Above this field, an exponential $j_c(B)$ dependence is found, typical for flux creep. This characteristic dependence corresponds in the logarithmic plot of Fig. 1 to the linear part of the $j_c(B)$ curves observed in a wide range of fields and temperatures. The field range between the two kinks dominated by weak links increases with decreasing temperature and at low temperatures, this range is extended up to the highest examined magnetic fields.

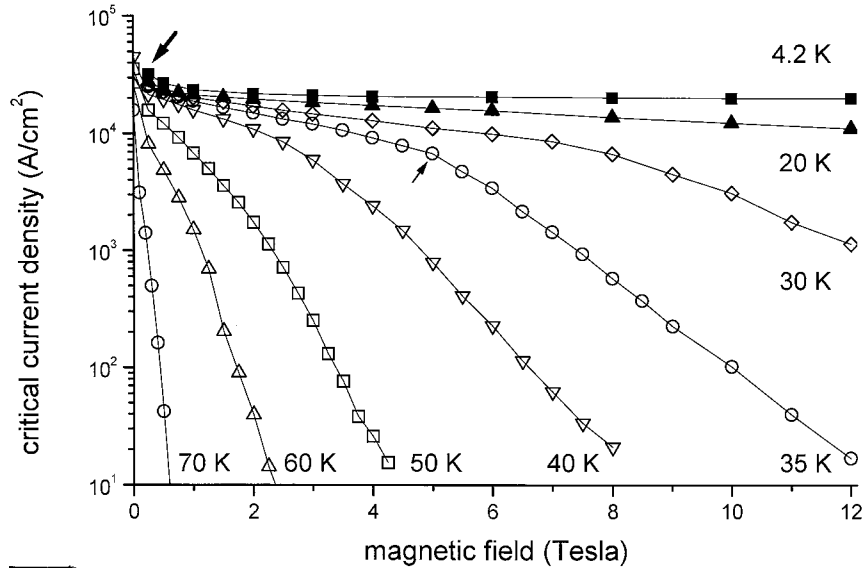

Fig. 1. Critical current density as a function of magnetic field, determined by transport measurements. A thick arrow points at the first kink and a thin one points at the second kink appearing at 35 K.

3.2. Microstructure of the split superconducting core

The microstructure of the split core was examined by a scanning electron microscope (SEM). Fig. 2a shows a survey of the surface. The quite rough separation method described above produced a surprisingly smooth surface. No cracks, terraces or grooves are observed over lengths of 4–6 mm. A

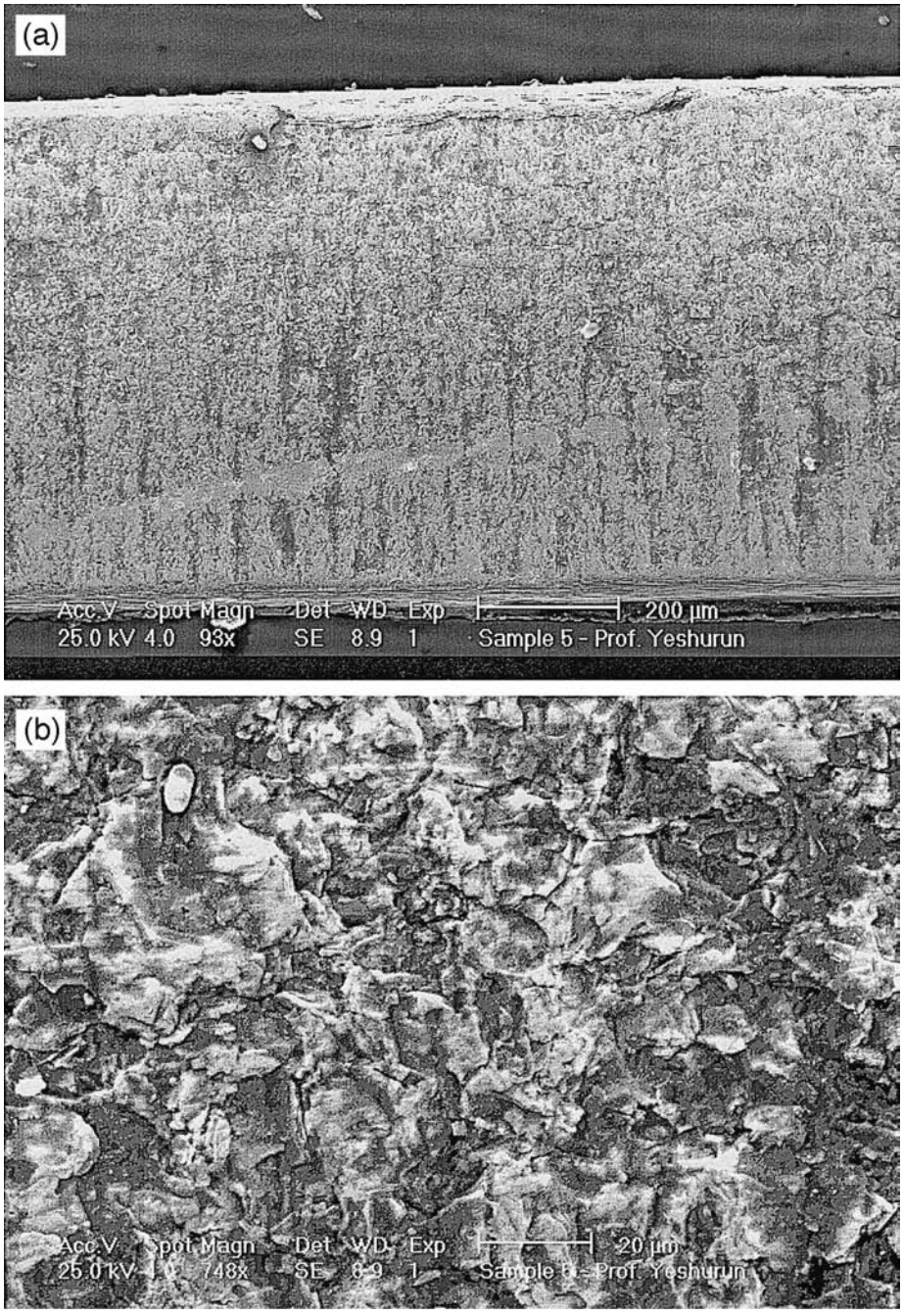

Fig. 2. Microstructure of the split core using SEM. (a) survey of the surface. (b) detailed view of the surface.

more detailed view with higher magnification is given in Fig. 2b. Colonies of about 20 μm diameter are in close contact and form a dense structure with a surface roughness of less than 1 μm.

To get more insight into the substructure of the colonies, the core was broken along its length and the fracture surfaces were examined. Fig. 3a,b show typical results. The colonies consist of plate-like grains of 10 μm diameter and 0.2 μm thickness, which are stacked upon each other along the common *c*-axis. The *c*-axis is oriented normal to the tape surface with a mean misalignment of about 5°. The predominant intercolony connections observed are *c*-axis twist boundaries formed by the partial overlap of the basal plane of adjacent colonies. Small angle *a*- and *b*-axis tilt boundaries that form the main structural element in the 'railway switch' model [6] for the current transport in the tapes were rarely found. Transport measurements on artificially synthesized *c*-axis twist boundaries between Bi-2212 single crystals reveal that this type of boundary forms strong links and does not suppress the intergrain critical current [22]. So the microstructure observed here supports the idea of a meandering current path over *c*-axis boundaries as proposed in the 'brick-wall' model [7–9].

3.3. Local magnetization measurements and field profiles on small samples

The properties of a small sample (2 mm × 0.7 mm) extracted from the tape, were investigated by local magnetization measurements in magnetic fields up to 1 T for different temperatures between 40 K and 80 K. The sample was placed on the Hall-probe array, in such a way that its bare surface was in contact with the probes and the silver sheath was furthest away from the detectors (see inset to Fig. 4).

In Fig. 4, typical magnetization loops are shown measured at 40 K by probes located at 35 and 155 μm from the sample's center. The width of the loop is largest in the center of the sample (the anomalous position of the peak described in Ref. [23] does not appear in our measurements), and decreases toward the edges, as expected from basic considerations based on a modified Bean model [24]. From the loops, induction profiles were determined at particular applied fields using the signals of the 11 Hall probes of the array. Fig. 5 shows such a profile, measured at 40 K and 3 kG in the descending part of the loop. The profile displays sharp peaks at the center of the sample, and close to its edges. The curvature of $B_z(x)$ is a result of demagnetization and is typical for platelet crystals in a perpendicular magnetic field [25].

The graph in Fig. 5 shows a fit of the experimental data to a calculation of B_z assuming a uniform bulk current and additionally, a surface current flowing in a 20 μm wide strip next to the edges. The values of the bulk current density j_b and the surface current density j_s that best fit the data are stated in the figure captions. Further calculations show that the bulk current varies between about 1×10^4 A/cm^2 at 0.3 T and 3.8×10^4 A/cm^2 in self field. These values are comparable with the critical current densities of 1.2×10^4 A/cm^2 (at 0.3 T) and 4.5×10^4 A/cm^2 (self field) determined at 40 K from transport measurements for the tapes (see Fig. 1). The induction profiles shown in Fig. 6a,b were measured at 80 K for two applied fields in the ascending branch of the magnetization loop. A significant bulk current was found to exist at fields below about 700 G, while surface currents seemingly dominate the field profiles for higher fields.

Other than fitting the data, we can determine the persistent currents using the inversion scheme. Before entering into the details of the computation, it is worthwhile to note that $4\pi/c \;\; J = \mathrm{d}B_z/\mathrm{d}x - \mathrm{d}B_x/\mathrm{d}z$, cannot be deduced from the induction profile, simply because $\mathrm{d}B_x/\mathrm{d}z$ cannot be neglected due to demagnetization enhanced by the geometry of the sample. It is therefore essential to use an inversion scheme similar to the one proposed by Wijngaarden et al. [26] and Brandt [27]. In this approach we assume the current is flowing in N vertical slices. Within each slice the current is homogeneous, and we assume symmetry of B_i^z (a value measured by a single Hall-probe) and antisymmetry of j_i around the middle of the sample. The symmetry of B_i^z is achieved by mirror imaging the B_i^z values of half the sample, thus limiting the number of slices by twice the number of probes located above one half of the sample (12 in this instance). The Biot-Savart integral is than written in a matrix form $B_i^z = \mathbf{M}_{ik} j_k$, where M_{ik} is a geometry-dependent matrix which can be analytically calculated. The matrix M_{ik} can

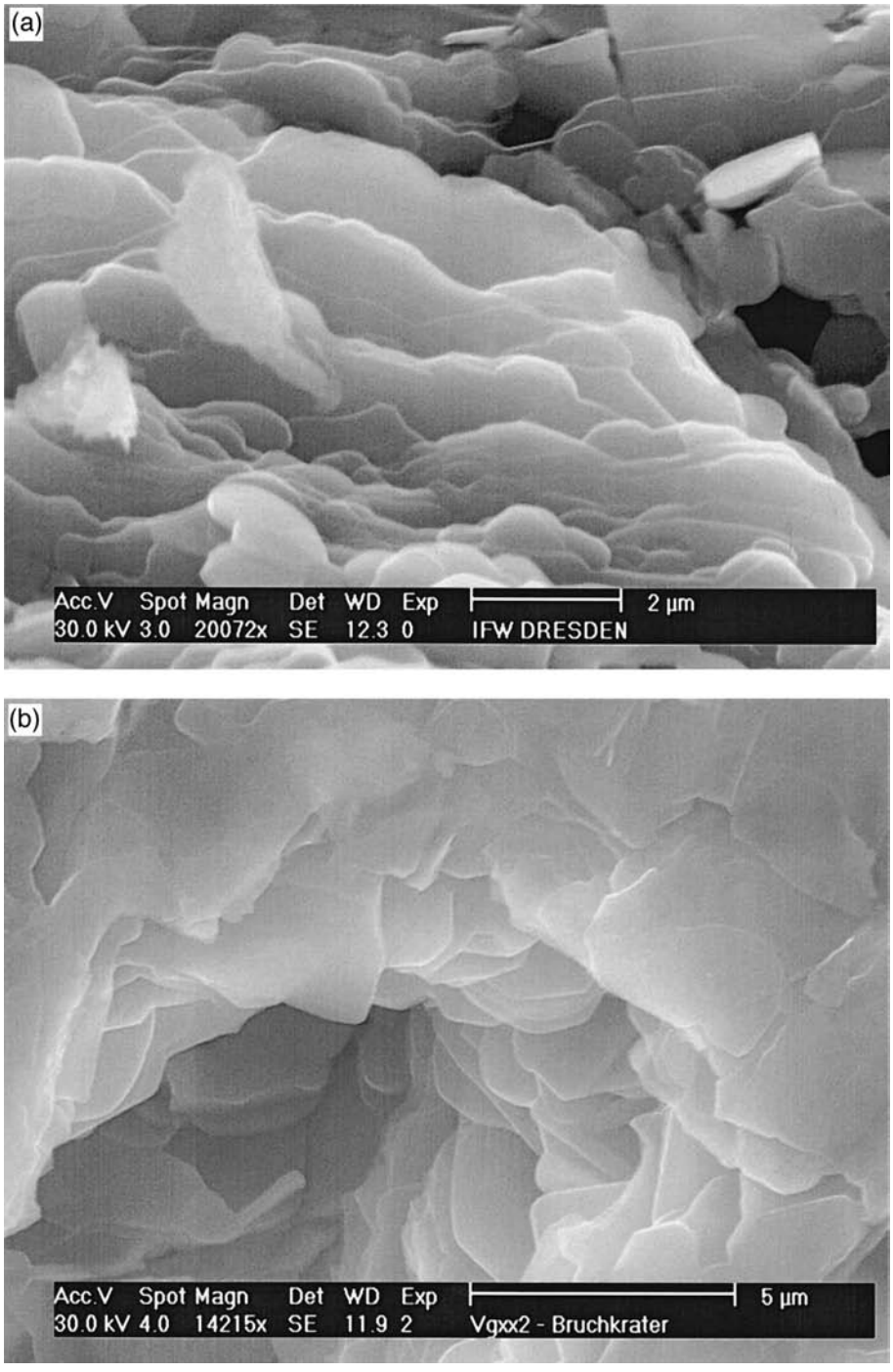

Fig. 3. Typical pictures of surfaces of fracture along the length of the sample.

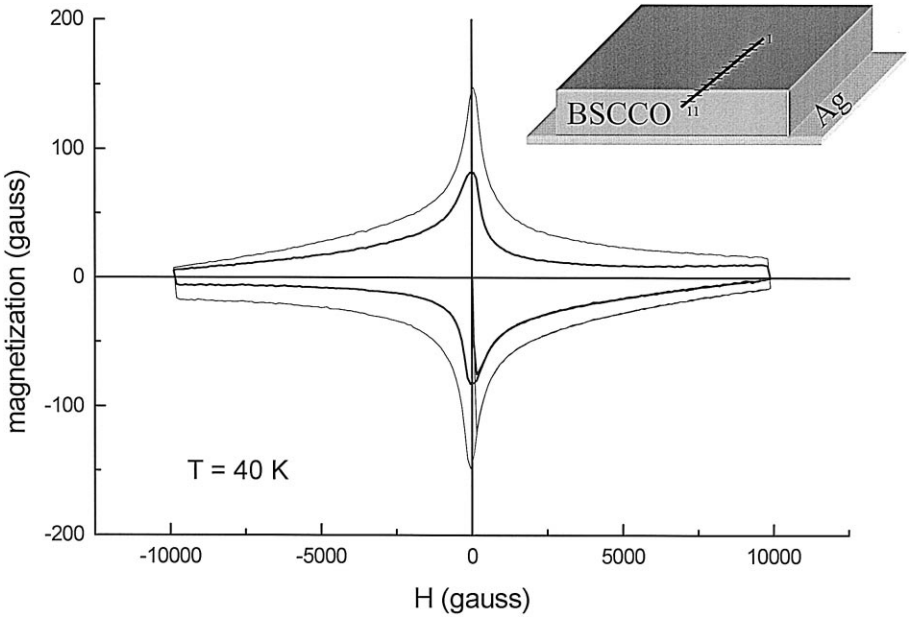

Fig. 4. Typical magnetization loops at 40 K at two different probes. The loops are measured by probes located 35 μm (outer loop) and 155 μm (inner loop) to the right of the sample's center. Inset shows configuration of Hall probe array in relation to the sample.

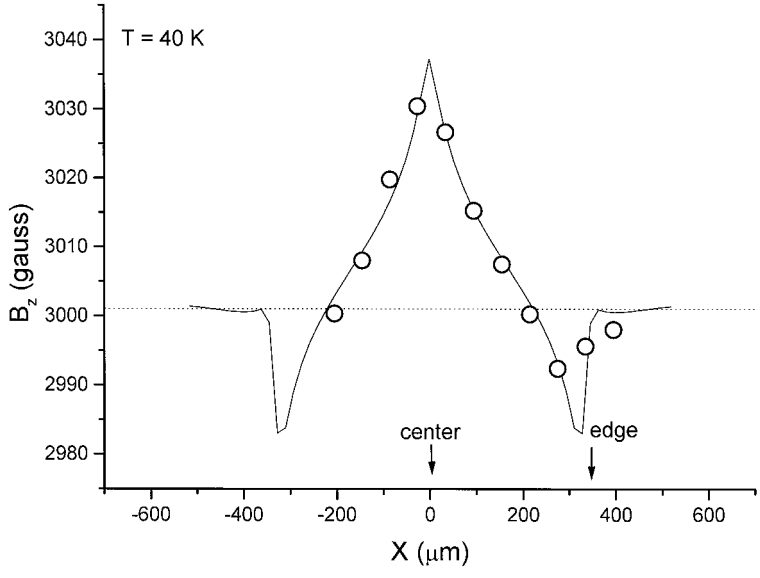

Fig. 5. Induction profile at 40 K in a descending field of about 3000 G. Data are depicted in open circles, the solid line is the fit to a combination of bulk and surface currents (see text) with: $J_{\text{bulk}} = 10^4$ A/cm^2, $J_{\text{surface}} = 3.4 \times 10^4$ A/cm^2. The size of the external field is shown by a dotted line.

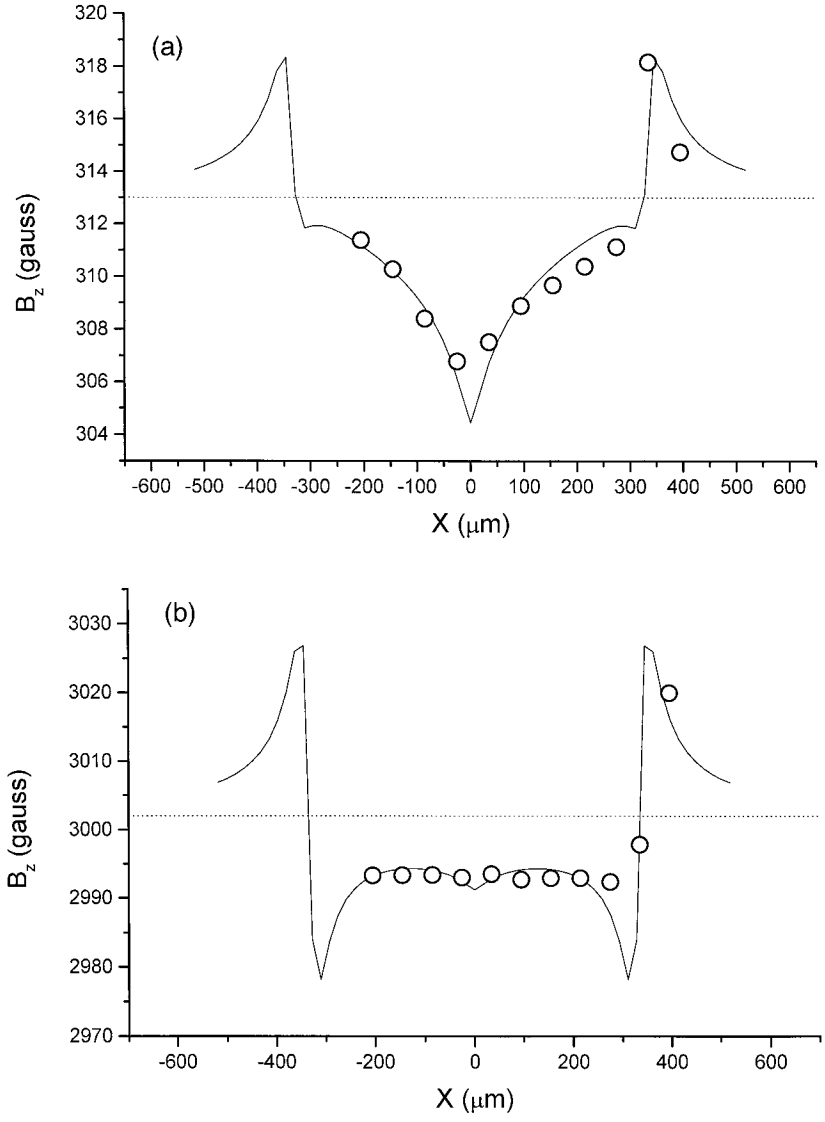

Fig. 6. Induction profiles at 80 K. Data are depicted in open circles, connected by the fit to a combination of bulk and surface currents. The size of the external field is shown by a dotted line. (a) At 300 G $J_{bulk} = 2160$ A/cm^2, and $J_{surface} = 8280$ A/cm^2, $T = 80$ K (see Fig. 5). (b) At 0.3 T a large part of the current flows within the grains resulting in an apparent surface current ($J_{bulk} = 1507$ A/cm^2, $J_{surface} = 7.6 \times 10^4$ A/cm^2, $T = 80$ K (see Fig. 5).

now be inverted, and j_k solved for. In Fig. 7, the current density distributions at 40 K and 80 K are shown in the remanent state for the case of ascending field.

It is interesting to note that the critical current density determined by magnetization measurements on the small sample agree roughly with that obtained for the tape by transport measurements not only at low temperatures, but also at 80 K in the remanent state: the experimental value for the transport critical density of 1.5×10^4 A/cm^2 at 77 K in self field is expected to reduce at 80 K by a factor of two on about 7.5×10^3 A/cm^2, whereas from the magnetization data a bulk current between 6.5×10^3 and

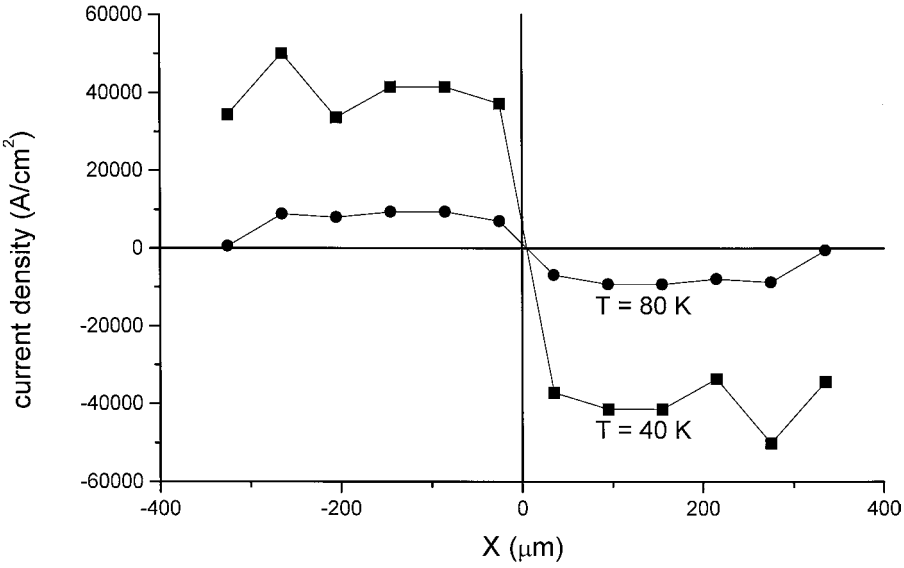

Fig. 7. Current density distributions derived using an inversion scheme (see text) at 40 K (squares) and 80 K (circles).

8×10^3 A/cm^2 was determined. This agreement gives us confidence that the properties of the small sample extracted from the tape are representative for the tape.

In local magnetization we have found no characteristic change in the critical transport current $j_c(H)$ of the tape (similar to the one appearing in Fig. 1) at 77 K in the range above 0.1 T, where the so-called

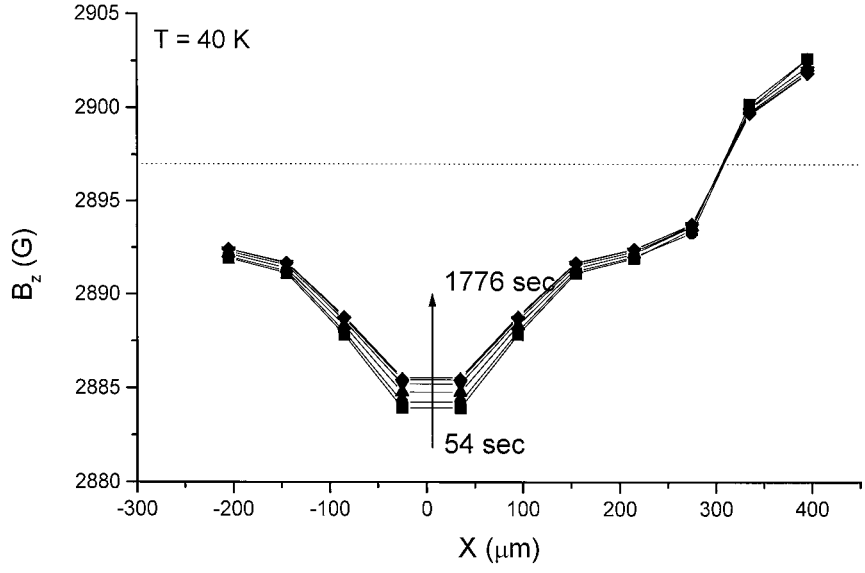

Fig. 8. Evolvement of the induction profile over time at 40 K and ascending field. In the center of the sample the induction increases as flux enters the sample. Near the edges flux exits the sample and the induction decreases. At the neutral line there is no change in the induction, and its value is equal to the external field (dotted line).

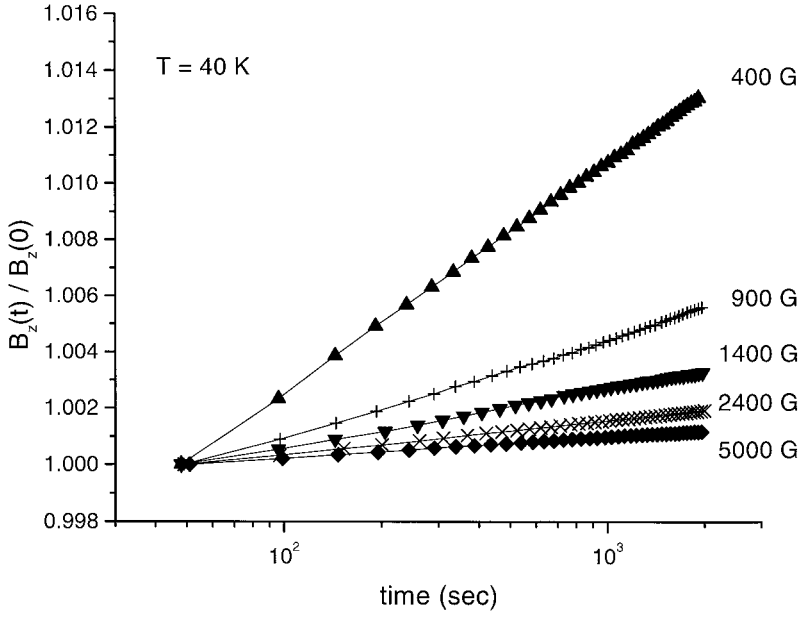

Fig. 9. The evolvement in time of the normalized induction at the probe closest to the center at 40 K and field ranging from 400 (triangles) to 5000 G (diamonds). The slope indicates the relaxation rate, and clearly this is larger for smaller fields.

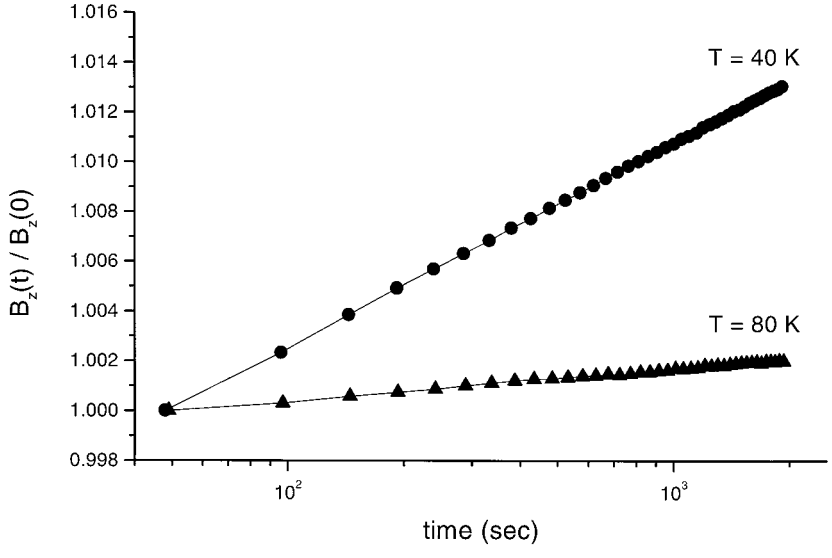

Fig. 10. The evolvement in time of the normalized induction at the probe closest to the center at 40 K (circles) and 80 K (triangles), both measured at 400 G.

surface currents dominate. It was assumed up to now that the whole range of the exponential $j_c(B)$ dependence is governed by flux creep and bulk pinning and that the current flows uniformly across the width of the grains. The results from the magnetic measurements lead us to a new interpretation of the data. At the region above the first kink (which covers most of our magnetic data at 40 K, but only the remanent field at 77 K) the current flows through the bulk—meaning that there exist links within the *ab* plane. At this region magnetic and transport data agree. At the region below the first kink, some of the links within the *ab* plane break. Current induced by the magnetic field will prefer to circulate within individual grains, the links between whom were broken. The current loops average each other out within the sample, but create a net current near the edges. Thus, an illusion of surface current is formed. In contrast, in transport measurements the current is forced to find outlets, which will enable it to cross the sample. This can be done if the current flows across links connecting different planes, as described by the 'brick wall' model [7–9]. Below the second kink the transport current flows in a layer close to the silver sheath, where the grains are better connected. One should notice, that the silver sheath is parallel to the surface glued to the Hall probe array and far from it, and thus current flow close to this layer cannot explain our results from magnetic measurements.

3.4. Measurement of the magnetic relaxation

The evolvement of the profile in time is shown in Fig. 8. The relaxation is most marked at the center of the sample, where the induction increases as flux enters the sample. Outside the sample the induction decreases, and at the neutral line there appears no change in the induction.

The time dependence of the magnetization is shown in Fig. 9, to be logarithmic in time. As the field increases the relaxation rate, $1/M_o\ \partial \ln\ M/\partial \ln\ t$, decreases and the slope becomes less steep.

The change in the induction during the same time interval is much slower at 80 K than at 40 K, as can be seen in Fig. 10. This is a consequence of the measurement time window. The relaxation at 80 K is much faster, therefore when the measurement commences (about 50 s after the field was ramped) most of the changes have already occurred. As a result, relaxation measurement cannot help discern between real surface currents, which should not relax over time, and apparent surface currents, resulting from the averaging of current loops within the grains, which should evolve in time.

4. Conclusions

We have shown and compared local magnetic measurements and global transport measurements of Bi-2223/Ag tapes. The two methods show a good agreement in the region where the current flows through the bulk. The methods diverge at high temperatures and relatively high fields. In these region the currents, induced by the magnetic field, prefer to flow within the grains, while the transport current must flow along the sample. We conclude that the 'brick wall' model aptly describes the flow of transport currents, but fails to describe the flow of currents induced by an external magnetic field.

Acknowledgements

We would like to thank Eli Zeldov for discussions and H. Shtrikman for growing the GaAs heterostructures. This research was partially supported by the Israel Science Foundations, by the Heinrich Hertz Minerva Center for High Temperature Superconductivity and by Bundesministerium für Bildung, Wissenschaft, Forschung und Technologie. Y.Y. acknowledges a support from the Ministry of Energy and Infrastructure and from the Ministry of Science and Technology.

References

[1] U. Balachandran, A.N. Iyer, R. Jammy, M. Chudzik, M. Lelovic, P. Krishnaraj, N.G. Eror, P. Haldar, IEEE Trans. Appl. Supercond. 7 (1997) 2207.
[2] K. Sato, K. Ohkura, K. Hayashi, M. Ueyama, J. Fujikami, T. Kato, Physica B 216 (1996) 258.
[3] T. Fahr, A. Hütten, W. Pitschke, C. Rodig, U. Schläfer, M. Schubert, P. Trinks, K. Fischer, in: H. Rogalla, D.H. Blank

(Eds.), Applied Superconductivity 1997, Proc. 3rd European Conf. on Appl. Supercond., EUCAS '97, 30 June–3 July, 1997, Eindhoven, Netherlands, IOP Publishing, Bristol, Vol. 2, 1997 p. 961.
[4] Q.Y. Hu, H.W. Weber, F.M. Sauerzopf, G.W. Schulz, R.M. Schalk, H.W. Neumüller, S.X. Dou, Appl. Phys. Lett. 65 (1994) 3008.
[5] H. Safar, J.H. Cho, S. Fleshler, M.P. Maley, J.O. Willis, J.Y. Coulter, J.L. Ullmann, P.W. Lisowski, G.N. Riley, M.W. Rupich, J.R. Thompson, L. Krusin-Elbaum, Appl. Phys. Lett. 68 (1996) 1853.
[6] B. Hensel, G. Grasso, R. Flükiger, Phys. Rev. B 51 (1995) 15456.
[7] A.P. Malozemoff, G.N. Riley, Jr., S. Fleshler, Q. Li, Proc. of SPA '97 Conf., Xi'an, China, March 6–8, 1997.
[8] L.N. Bulaevskii, J.R. Clem, L.I. Glazman, A.P. Malozemoff, Phys. Rev. B 45 (1992) 2545.
[9] L.N. Bulaevskii, L. Daemen, M. Maley, J. Coulter, Phys. Rev. B 48 (1993) 13798.
[10] G. Fuchs, T. Staiger, P. Verges, K. Fischer, A. Gladun, Applied Superconductivity 1995, Inst. Phys. Conf. Ser. No. 148, Vol. 1, D. Dew-Hughes (Ed.), IOP Publishing, Bristol, 1995, p. 443.
[11] Th. Staiger, G. Fuchs, P. Verges, K. Fischer, L. Schultz, IEEE Trans. Appl. Supercond. 7 (1997) 1347.
[12] A.E. Pashitski, A. Polyanskii, A. Gurevich, J.A. Parrell, D.C. Larbalestier, Physica C 246 (1995) 133.
[13] J.A.J. Paasi, M.J. Lahtinen, V. Plechacek, Physica C 242 (1995) 267.
[14] D.C. Larbalestier, Y. Feng, X.Y. Cai, H. Edelman, E.E. Hellstrom, J.A. Parrell, Y.S. Sung, A. Umezawa, Proc. 7th Int. Workshop on Critical Currents in Superconductors, Alpbach, Austria, 24–27 January 1994, H.W. Weber (Ed.), World Scientific, Singapore, 1994, p. 82.
[15] G. Grasso, B. Hensel, A. Jeremie, R. Flükiger, Physica C 241 (1994) 45.
[16] E. Zeldov, A.I. Larkin, V.B. Geshkenbein, M. Konczykowski, D. Majer, B. Khaykovich, V.M. Vinokur, H. Shtrikman, Phys. Rev. Lett. 73 (1994) 1428.
[17] Y. Abulafia, A. Shaulov, Y. Wolfus, R. Prozorov, L. Burlachkov, Y. Yeshurun, D. Majer, E. Zeldov, Y.M. Vinokur, Phys. Rev. Lett. 75 (1995) 2404.
[18] Y. Abulafia, A. Shaulov, Y. Wolfus, R. Prozorov, L. Burlachkov, Y. Yeshurun, D. Majer, E. Zeldov, H. Wühl, V.B. Geshkenbein, Y.M. Vinokur, Phys. Rev. Lett. 77 (1996) 1596.
[19] D. Majer, E. Zeldov, H. Shtrikman, M. Konczykowski, Proc. of the Workshop Coherence in High Temperature Superconductors, Herzlia, Israel, 1–3 May 1995, G. Deutscher, A. Revcolevschi (Eds.), World Scientific, Singapore, 1996, p. 271.
[20] K. Fischer, A. Hütten, E. Müller, H.-P. Trinks, T. Staiger, B. Wolf, Advances in Superconductivity VIII, H. Hayakawa, Y. Enomoto (Eds.), Vol. 2, Springer, Tokyo, 1996, p. 843.
[21] M. Lelovic, P. Krishnaraj, N.G. Eror, U. Balachandran, Physica C 242 (1995) 246.
[22] Li Qiang , Y. Tsay, Y. Zhu, M. Suenaga, G. Gu, N. Koshizuka, IEEE Trans. Appl. Supercond. 7 (1997) 1584.
[23] M.R. Koblischka, L. Pust, A. Galkin, P. Nálevka, Appl. Phys. Lett. 70 (1997) 514.
[24] R. Prozorov, M. Konczykowski, B. Schmidt, Y. Yeshurun, A. Shaulov, C. Villard, G. Koren, J. Appl. Phys. 76 (1995) 7621.
[25] E. Zeldov, J.R. Clem, M. McElfresh, M. Darwin, Phys. Rev. B 49 (1994) 9802.
[26] R.J. Wijngaarden, H.J.W. Spoelder, R. Surdeanu, R. Griessen, Phys. Rev. B 54 (1996) 6742.
[27] E.H. Brandt, Phys. Rev. B 46 (1992) 8628.